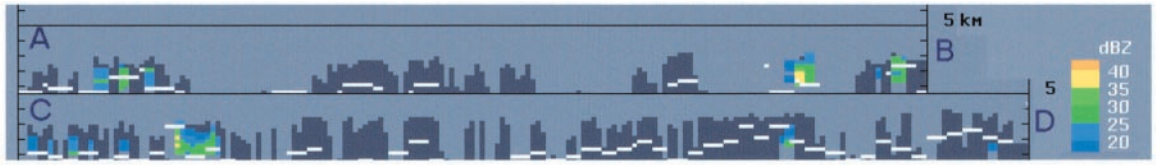

Fig. 5. Vertical cross section along the lines AB and CD in Fig. 2. The dark gray areas represent clouds. The vertical extent of the clouds is converted from the VIRS-measured cloud-top temperatures. The colors represent the precipitation reflectivity in dBZ as measured by the TRMM radar. The white line is the brightness temperature of the TMI 85-GHz vertical polarization (T_{85}), plotted at the altitude of that temperature. A lower T_{85} value is represented as greater height of the white line, and in nonprecipitating clouds it means greater cloud water content. The T_{85} and actual cloud-top temperature have different physical meanings.

and secondary ice generation in clouds (*23*, *24*). Air pollution must be an important factor in determining the precipitation amounts in the Snowy Mountains (east of box 4 in Fig. 2) because it has been observed that most of the winter precipitation events in that region come from clouds with temperature at the tops between −4° and −13°C (*25*). Interestingly, a decreasing trend of the snow cover in the Snowy Mountains was reported for the period 1897–1991 (*25*). However, trend analyses of snow, winter temperature, and total winter rainfall for the period 1910–91 showed statistically insignificant decreases in all three parameters (*26*).

The satellite data provide evidence connecting urban and industrial air pollution to the reduction of precipitation, pinpointing both the sources and the affected clouds. This has become possible with the newly acquired capabilities to observe both cloud microstructure and precipitation over large areas with TRMM satellite observations. It might seem strange that some of the most prominent pollution signatures occur in Australia, which is probably the least polluted inhabited continent. The pollution is perhaps most evident in Australia because it is seen against a background of pristine clouds, whereas in most other places the clouds are already polluted on a very large scale. Such results might indicate that human activity may be altering clouds and natural precipitation on a global scale.

References and Notes

1. P. V. Hobbs and L. F. Radke, *Science* **163**, 279 (1969).
2. Y. J. Kaufman and R. S. Fraser, *Science* **277**, 1636 (1997).
3. P. Squires, *Tellus* **10**, 256 (1958).
4. P. R. Jonas and B. J. Mason, *Q. J. R. Meteorol. Soc.* **100**, 286 (1974).
5. J. Warner, *J. Appl. Meteorol.* **7**, 247 (1968).
6. D. Rosenfeld and I. Lensky, *Bull. Am. Meteorol. Soc.* **79**, 2457 (1998).
7. TRMM was launched on 28 November 1997 as a cooperative project of the National Aeronautics and Space and Administration (NASA) and the National Space Development Agency of Japan (NASDA). The TRMM data are available at http://daac.gsfc.nasa.gov/CAMPAIGN_DOCS/hydrology/hd_trmm_intro.html.
8. D. Rosenfeld, *Geophys. Res. Lett.* **26**, 3105 (1999).
9. R. Gunn and B. B. Phillips, *J. Meteorol.* **14**, 272 (1957).
10. R. C. Eagen, P. V. Hobbs, L. F. Radke, *J. Appl. Meteorol.* **13**, 535 (1974).
11. R. R. Braham Jr., *Meteorol. Monogr.* **18**, 141 (1981).
12. D. B. Johnson, *J. Atmos. Sci.* **39**, 448 (1982).
13. D. F. Gatz, *J. Appl. Meteorol.* **18**, 1245 (1979).
14. E. Jauregui and E. Romales, *Atmos. Environ.* **30**, 3383 (1996).
15. R. S. Cerveny and R. C. Balling Jr., *Nature* **394**, 561 (1998).
16. J. A. Coakley Jr., R. L. Bernstein, P. A. Durkee, *Science* **237**, 1020 (1987).
17. L. F. Radke, J. A. Coakley Jr., M. D. King, *Science* **246**, 1146 (1989).
18. B. A. Albrecht, *Science* **245**, 1227 (1989).
19. Emission data obtained from Flinders Power, Port Augusta, South Australia, Australia.
20. D. Rosenfeld and G. Gutman, *J. Atmos. Res.* **34**, 259 (1994).
21. Information about the TRMM ground validation program is available at http://trmm.gsfc.nasa.gov/trmm_office/field_campaigns/field_campaigns.html.
22. R. Oki *et al.*, *Mar. Technol. Soc. J.* **32**, 13 (1999).
23. S. C. Mossop and J. Hallett, *Science* **186**, 632 (1974).
24. A. Rangno and P. V. Hobbs, *Q. J. R. Meteorol. Soc.* **120**, 573 (1994).
25. B. Harasymiw and J. McGee, *Snowy Precipitation Enhancement Project: A Proposal to Evaluate Feasibility of Increasing Snow Precipitation over the Snowy Mountains Area* (Snowy Mountains Hydroelectric Authority, Cooma, Australia 1993), appendix B.
26. A. L. Duus, *Aust. Meteorol. Mag.* **40**, 195 (1992).

27. I thank all the members of the TRMM team, too numerous to mention individually, for all their hard work to make the satellite a reality and the data of such high quality. The NOAA AVHRR data were obtained from the NOAA Satellite Active Archive. I also thank A. Gingis of Australian Management Consolidated Pty., Ltd. for assisting in this study and W. L. Woodley for help with the manuscript.

5 November 1999; accepted 10 January 2000

An Archaeal Iron-Oxidizing Extreme Acidophile Important in Acid Mine Drainage

Katrina J. Edwards,[1,2]* Philip L. Bond,[1] Thomas M. Gihring,[1] Jillian F. Banfield[1]

A new species of Archaea grows at pH ~0.5 and ~40°C in slime streamers and attached to pyrite surfaces at a sulfide ore body, Iron Mountain, California. This iron-oxidizing Archaeon is capable of growth at pH 0. This species represents a dominant prokaryote in the environment studied (slimes and sediments) and constituted up to 85% of the microbial community when solution concentrations were high (conductivity of 100 to 160 millisiemens per centimeter). The presence of this and other closely related *Thermoplasmales* suggests that these acidophiles are important contributors to acid mine drainage and may substantially impact iron and sulfur cycles.

The oxidative dissolution of metal sulfide minerals causes the formation of acid mine drainage (AMD) and plays an important role in the geochemical sulfur cycle. Sulfides (primarily pyrite, FeS_2) that are exposed to air and water through geological or mining activities undergo oxidative dissolution and generate sulfuric acid by the reaction $FeS_2 + 14Fe^{3+} + 8H_2O \rightarrow 15Fe^{2+} + 2SO_4^{2-} + 16H^+$ (*1*). Mining and extraction mobilizes ~150×10^{12} g of sulfur per year, contributing ~50% to the net river transport of sulfate to the ocean, which is about half of the sulfate input into the ocean (*2*).

Microorganisms accelerate the rate of pyrite dissolution through regeneration of Fe^{3+} (*1*, *3*), the primary pyrite oxidant at low pH (*4*–*6*). At Iron Mountain, an AMD site in northern California, the iron-oxidizing bacterium *Thiobacillus ferrooxidans*, previously thought to be the most important iron-oxidizing species, played a minor role in pyrite oxidation (*7*, *8*). Instead, Archaea constituted a large proportion (>50%) of the prokaryote population at important sites of acid generation during the dry summer and fall months

[1]Department of Geology and Geophysics, University of Wisconsin–Madison, 1215 West Dayton Street, Madison, WI 53706, USA. [2]Woods Hole Oceanographic Institute, Department of Marine Chemistry and Geochemistry, Woods Hole, MA 02543, USA.

*To whom correspondence should be addressed at Woods Hole Oceanographic Institute, Department of Marine Chemistry and Geochemistry, Woods Hole, MA 02543, USA. E-mail: kedwards@whoi.edu

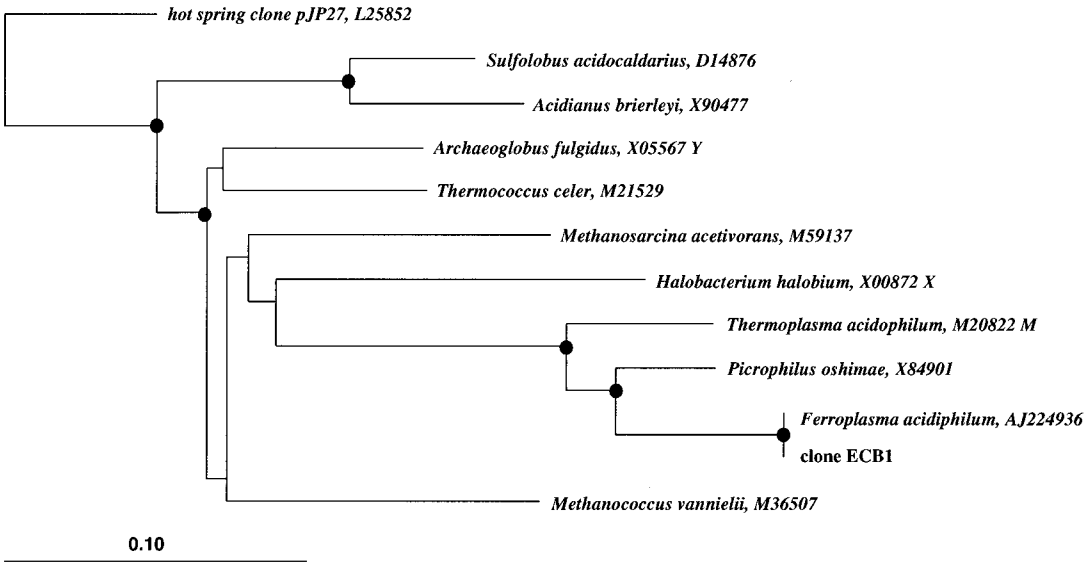

Fig. 1. Phylogenetic relationship of clone ECB1 within the Archaeal domain based on comparison of partial 16*S* ribosomal DNA sequences. Clone sequences were aligned to representative sequences from the Ribosomal Database Project [RDP (*25*)] and GenBank (*26*) databases. Phylogenetic analysis was performed with the ARB software package (*27*). Sequences were aligned and reduced to 819 comparable positions with a filter created in ARB. A dendogram was constructed in ARB by evolutionary distance (neighbor joining) and compared to inference by maximum likelihood [fastDNAml; RDP (*25*)]. Accession numbers are shown for the comparison sequences that were obtained from the RDP (*25*). Branch points on the dendogram are indicated by filled circles when supported by both evolutionary distance and maximum likelihood analyses.

(*8*). Here we describe the isolation, identification, and physiology of an Archaeon from Iron Mountain and the ecological niche it, and closely related Archaea, occupy.

We started enrichment cultures with sediments and mine water collected in July 1997 from the B-drift at the Richmond 5-way. The 5-way is a site ~500 m into the mountain, situated within the remaining pyrite ore-body at a junction between five tunnels. Temperatures at the Richmond 5-way are ~40°C, and the pH of the waters is 0 to 1 (*8*). The low-pH conditions at Iron Mountain support extremely high metal concentrations in solutions; iron has been measured as high as 111 g liter^{-1}, and copper, arsenic, cadmium, and zinc all have been measured in the tens to tenths of grams per liter range (*9*). Specific conductance at the time of collection was ~120 mS cm^{-1} (*8*). We grew enrichment cultures at 37°C in pH 1 medium (*10*), using pyrite sediments as the energy source. We performed DNA extractions and constructed clone libraries for two of the enrichment cultures and sequenced representative clones (*11*). A high proportion of the clones formed a monophyletic cluster with *Ferroplasma acidiphilum* (*12*), an iron-oxidizing chemolithotrophic, autotrophic Archaeon within the order *Thermoplasmales* (Fig. 1). The *Thermoplasmales* are acidophilic Archaea that possess only a single, peripheral (cytoplasmic) membrane (*12*). Subsequently, from an enrichment culture, an isolate (fer1; Fig. 2) was obtained by serial dilution in pH 1.5 medium (*10*) that was supplemented with 20 g liter^{-1} $FeSO_4 \cdot 7H_2O$ and 0.02% yeast extract. Fluorescent in situ hybridizations [FISH (*13*)] with a probe designed for the *Ferroplasma* cluster FER656 (*13*) confirmed that the isolate was a *Ferroplasma* species.

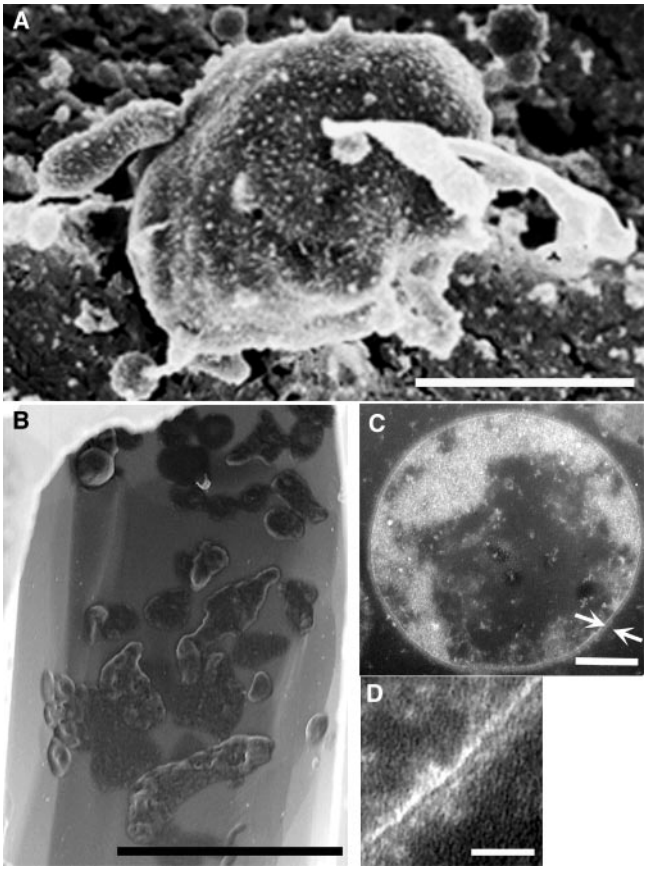

Fig. 2. Scanning (SEM) and transmission (TEM) electron micrographs of *F. acidarmanus* isolate fer1. (**A**) Cryo-SEM (bar, 500 nm). Fer1 cells in late log growth were prepared for high-pressure cryoscanning electron microscopy as described (*28*). Cells were viewed with a Hitachi S900 scanning electron microscope operated at 2 kV, on a Gatan cryostage. Irregular-sized and -shaped cellular protrusions that can be seen are inferred to be budding sections of the cell. (**B**) SEM micrograph (bar, 5 μm) of a microcolony of fer1 cells within a dissolution pit on a pyrite surface. Samples were prepared and examined as described (*29*). When grown with sulfide minerals (pyrite, marcasite, and arsenopyrite) as the energy source, fer1 cells preferentially grow attached to the mineral surface relative to growth in free suspension. (**C**) TEM image of fer1 (bar, 150 nm), and (**D**) higher magnification (bar, 25 nm) of the area shown in (C) with arrows, illustrating the single, peripheral membrane surrounding the cell that gives rise to the irregular, pleomorphic morphology (A and B). Samples were prepared for TEM as described (*12*) and viewed with a Zeiss 10CA at 60 kV.

Although fer1 is phylogenetically similar to *F. acidiphilum* (Fig. 1), it is physiologically distinct. Both fer1 and *F. acidiphilum* require yeast extract for growth, but fer1 is also able to grow heterotrophically on yeast extract as the sole energy source (*14*), whereas *F. acidiphilum* cannot (*12*). Fer1 is able to grow between pH 0 and 2.5, with a growth optimum at pH 1.2 (*14*). In contrast, *F. acidiphilum* grows over a more restricted pH

range, has a higher pH optimum [optimum 1.7; range, 1.3 to 2.2 (*12*)], and doubles at about one-third the rate at optimal pH [~32 hours (*12*)]. Hence, we suggest a new species name, *acidarmanus* for fer1, within the genus *Ferroplasma*.

In order to determine the proportion of *F. acidarmanus* at Iron Mountain, we collected sediment and slime samples from the Richmond 5-way in November 1998 for analysis using FISH (*13*). We collected samples for FISH from the same localities collected from in July 1997 for enrichment cultures (above). In the new samples, 85 ± 7% of the total population in a biofilm (Fig. 3) associated with the sediments hybridized with the *Ferroplasma* genus–specific probe FER656. The remainder of this biofilm was composed of eukaryotic filaments; hence, essentially the entire prokaryote population was *F. acidarmanus*. This species is thus likely to be the Archaeon that was found in high abundance in sediment samples (*8*). Further analysis during 1999 confirmed that while the microbial diversity varies spatially and seasonally, *Ferroplasma* species remained a persistent and often dominant microbial constituent at the Richmond 5-way (*15*).

Microbial populations at subsurface AMD sites are typically poorly studied relative to run-off waters (*7*) because of the greater difficulty associated with sampling disused and hazardous underground regions. Two other recent studies have identified closely related *Thermoplasmales* that thrive in similar conditions. One is the previously mentioned *F. acidiphilum* isolate, obtained from a semi-industrial bioleaching reactor in Eastern Europe [Kazakhstan (*12*)]. In the other study (Chile; no isolate was obtained), *Thermoplasmales* were the predominate phylotype in a bioleaching reactor when it was operated under high-sulfate (low-pH) conditions (*16*). The high metal and sulfate conditions under which some bioleaching reactors are operated may be more representative of highly concentrated subsurface AMD sites than the diluted run-off waters that are more commonly studied. Highly concentrated, acidic solutions clearly enrich for these Archaea, both in the environment and in some bioleaching reactors, suggesting that they may be prevalent at subsurface sites. It is unclear how these closely related Archaea that readily lyse in neutral-pH solutions (*12*, *14*) come to be globally distributed. Current theories for distributing microorganisms would not apply to obligate acidophiles such as these (*17*).

How microorganisms are able to withstand extremely low pH is still uncertain. Membrane characteristics are believed to be critical features that allow Archaea to thrive in many hostile environments (*18*). It is notable that at Iron Mountain, where the lowest naturally occurring pH conditions have been reported to date (*9*), the Archaea that thrive lack cell walls entirely (*12*) (Fig 2). This suggests that the cytoplasmic membrane composition and construction are key factors for extreme acid tolerance. Only two other organisms, both *Thermoplasmales* within the genus *Picrophilus*, are capable of growth at pH 0 (*19*, *20*), the lowest pH recorded to support life. However, their abundance in the environment from which they were cultured is yet unknown.

Acidophily is a ubiquitous trait among the *Thermoplasmales*, yet they are not known to be important contributors to AMD production. Results of this work suggest that although extremophiles are often confined to sites of small geographic extent (such as hot springs and hydrothermal vents), the physiological function and environmental abundance of these Archaea indicate that they may substantially impact global cycling of iron and sulfur.

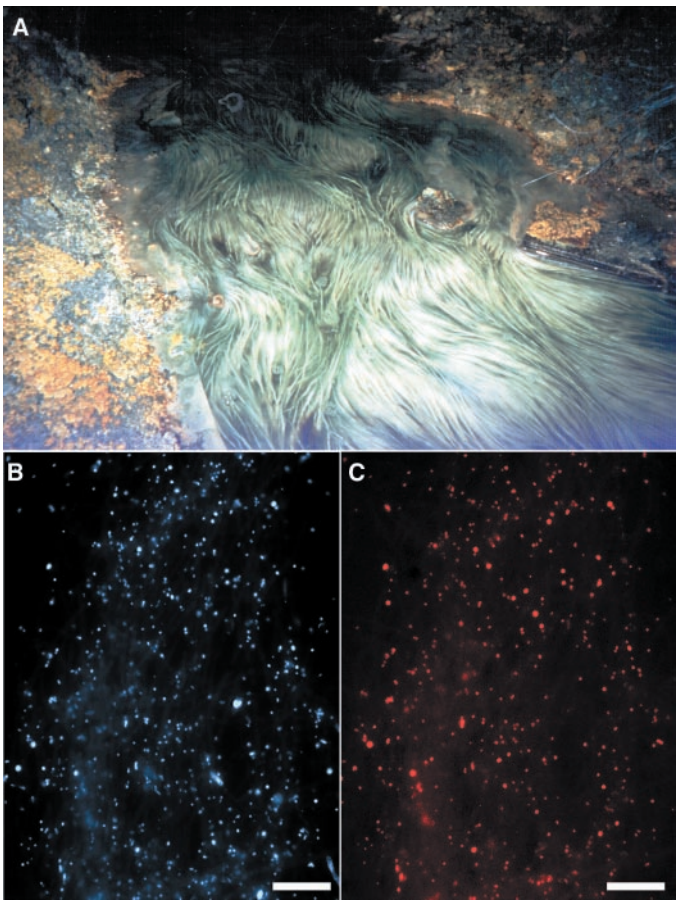

Fig. 3. Examples of the type of biofilm material used to determine the proportion of *F. acidarmanus*. (**A**) Stream at B-drift (~1 m across). The biofilm is anchored within pyritic sediments and forms dense slime streamers in most subsurface (tunnel) waters during the summer and fall months at the Richmond 5-way. (**B**) DAPI (4′,6′-diamidino-2-phenylindole)–stained microbial cells from B-drift slime streamers shown in (A). Bar (B and C), 10 μm. (**C**) Cells hybridized with the FER656 probe, from the same field of view as (B). To determine the proportion of cells that hybridized with FER656, counts were made for hybridized cells (*13*) versus cells stained with DAPI, (*30*) for four fields of view (0.04 mm^2) per well; counts were made for four separate wells.

References and Notes

1. D. K. Nordstrom and G. Southham, in *Geomicrobiology: Interactions Between Microbes and Minerals*, J. F. Banfield and K. H. Nealson, Eds. (Mineralogical Society of America, Washington, DC, 1997), vol. 35, pp. 361–390.
2. P. Brimblecombe, C. Hammer, H. Rodhe, A. Ryaboshapko, C. F. Boutron, in *Evolution of the Global Biogeochemical Sulphur Cycle*, P. Brimblecombe and A. Y. Lein, Eds. (Wiley, New York, 1989), pp. 77–121.
3. M. P. Silverman and H. L. Ehrlich, *Adv. Appl. Microbiol.* **6**, 153 (1964).
4. M. A. Williamson and J. D. Rimstidt, *Geochim. Cosmochim. Acta* **58**, 5443 (1994).
5. C. O. Moses, D. K. Nordstrom, J. S. Herman, A. L. Mills, *Geochim. Cosmochim. Acta*. **51**, 1561 (1987).
6. G. W. Luther III, *Geochim. Cosmochim. Acta*. **51**, 3193 (1987).
7. M. O. Schrenk, K. J. Edwards, R. M. Goodman, R. J. Hamers, J. F. Banfield, *Science* **279**, 1519 (1998).
8. K. J. Edwards, T. M. Gihring, J. F. Banfield, *Appl. Environ. Microbiol.* **65**, 3627 (1999).
9. D. K. Nordstrom and C. N. Alpers, *Proc. Natl. Acad. Sci. U.S.A.* **96**, 3455 (1999).
10. K. J. Edwards, M. O. Schrenk, R. Hamers, J. F. Banfield, *Am. Mineral.* **83**, 1444 (1998).
11. DNA extractions were performed as described (*21*), except that freeze (−70°C)-thaw (65°C) cycles were substituted for bead beating. The microbial community 16*S* ribosomal RNA genes were amplified by polymerase chain reaction, and these were cloned for analysis. Fifty-two clones were analyzed by restriction fragment length polymorphism (*22*). Representatives of dominant patterns were sequenced at the University of Wisconsin Biotechnology Center with an Automated DNA Sequencer (Applied Biosystems 377XL).
12. O. V. Golyshina *et al.*, *Int. J. Syst. Bacteriol.*, in press.
13. All material used for FISH was fixed in 4% paraformaldehyde in 1× phosphate-buffered saline (PBS) buffer (0.137 M NaCl, 0.005 M $NaHPO_4 \cdot 7H_2O$, 0.003 M KCl, 0.001 M KH_2PO_4), pH 7.3, for 2 hours. Fixed cells were washed and resuspended in a 1:1 ethanol: 1× PBS buffer and homogenized by vortexing before spotting 10 μl onto wells of a gelatin-coated (0.25%), multiwelled slide (Electron Microscopy Sciences). Hybridizations were carried out in buffer [0.9 M NaCl, 20 mM tris-HCl (pH 7.4), 0.01% SDS], 25 to 50 ng of oligonucleotide probe (synthesized at the University of Wisconsin Biotechnology Center), and formamide (25% for FER656; determined empirical-

ly). Samples were incubated in a buffer-equilibrated humidity chamber at 46°C for 90 min, then rinsed and immersed in wash buffer [20 mM tris-HCl (pH 7.4), 0.01% SDS, 5 mM EDTA, 0.9 M to 7 mM NaCl (*23*)] for 15 min at 48°C. Slides were rinsed in distilled water, air dried, and mounted with Vectashield (Vectashield Laboratories) for viewing. Enrichment cultures were used to determine optimal stringency for hybridization with FER656 (5′-CGTTTAACCTCAC-CCGATC-3′). The isolate fer1 was used as the positive control for hybridizations with FER656. Bacterial cultures used for negative FER656 hybridization controls included *T. ferrooxidans* (American Type Culture Collection 19859), *Acidimicrobium ferrooxidans* [German Collection of Microorganisms and Cell Cultures (DSMZ) 10331], *Acidiphilium* strain SJH (courtesy of B. Goebel), and *Escherichia coli* (JM109; purchased from Promega, WI). Bacterial and *Ferroplasma* cells in enrichment cultures were also used as controls; bacteria (*Leptospirillum ferrooxidans* and *Thiobacillus caldus*) were hybridized with BAC338 (*8*) (20% formamide).

14. For determination of generation times, 20 ml of medium (*10*) with 20 g liter^{-1} $FeSO_4 \cdot 7H_2O$ and 0.02% yeast extract were adjusted to the appropriate pH with H_2SO_4 and inoculated with 0.2 to 0.5 ml of a stationary phase culture. The pH electrode (Orion) was calibrated with commercially purchased standards for pH 1, 2, and 3 (Fisher Scientific) and with 0.146 M (pH 0.86), 0.734 M (pH 0.09), and 1.497 M (pH −0.38) H_2SO_4 reference solutions (*24*). Growth was determined by making direct cell counts with a Petroff-Hausser Counter (Fisher Scientific). Growth was not sustained above pH 2.5 or below 0. Comparable growth on 0.02% yeast extract in the absence of pyrite or $FeSO_4 \cdot 7H_2O$ is attained at pH 1.2.
15. P. L. Bond, S. P. Smirga, J. F. Banfield, unpublished data.
16. M. Vasquez, E. R. B. Moore, R. T. Espejo, *FEMS Microbiol. Lett.* **173**, 183 (1999).
17. J. T. Staley, *ASM News* **65**, 681 (1999).
18. J. L. van de Vossenberg and A. J. Driessen, *Extremophiles* **2**, 163 (1998).
19. C. Schleper *et al.*, *J. Bacteriol.* **177**, 7050 (1995).
20. C. Schleper, G. Puehler, H. P. Klenk, W. Zillig, *Int. J. Syst. Bacteriol.* **46**, 814 (1996).
21. S. M. Barns, R. E. Fundyga, M. W. Jeffries, N. R. Pace, *Proc. Natl. Acad. Sci. U.S.A.* **91**, 1609 (1994).
22. P. Hugenholtz, B. M. Goebel, N. R. Pace, *J. Bacteriol.* **180**, 4765 (1998).
23. R. Lathe, *J. Mol. Biol.* **183**, 1 (1985).
24. D. K. Nordstrom, C. N. Alpers, C. J. Ptacek, *Environ. Sci. Technol.* **34**, 254 (1999).
25. B. L. Maidak *et al.*, *Nucleic Acids Res.* **25**, 109 (1997).
26. D. A. Benson, M. S. Boguski, D. J. Lipman, J. Ostell, B. F. Ouellette, *Nucleic Acids Res.* **26**, 1 (1998).
27. Distributed by W. Ludwig and O. Strunk, University of Munich.
28. W. W. Barker, S. A. Welch, S. Chu, J. F. Banfield, *Am. Mineral.* **83**, 1551 (1998).
29. K. J. Edwards, thesis, University of Wisconsin–Madison (1999).
30. J. Kapuscinski, *Biotech. Histochem.* **70**, 220 (1995).
31. We thank D. K. Nordstrom, E. A. Webb, and the reviewers for their comments and P. Golyshin for providing us with his unpublished manuscript. We thank L. Kerr and Y. Chen for assistance with electron microscopy. We also thank Iron Mountain Mine for site access and Stauffer Management for providing assistance. Supported by NSF grant CHE-9521731.

9 November 1999; accepted 27 January 2000

Seismic Images of the Far Side of the Sun

C. Lindsey[1]* and D. C. Braun[1,2]

Images of an active region on the far side of the sun were derived by applying seismic holography to recent helioseismic observations from space. Active regions are the centers of energetic phenomena such as solar flares and coronal mass ejections, whose resulting electromagnetic and particle radiation interfere with telecommunications and power transmissions on Earth and can pose significant hazards to astronauts and spacecraft. Synoptic seismic imaging of far-side solar activity will now allow anticipation of the appearance of large active regions more than a week ahead of their arrival on the east solar limb.

Forecasts of space weather would be greatly improved by the ability to monitor active regions on the far side of the sun. Active regions on the near solar surface produce flares that affect spacecraft, cause surges in electrical power grids, and inhibit telecommunications. Because the sun rotates rapidly, with a synodic period of 27 days, flaring regions can appear suddenly on the east solar limb, affecting space weather in the terrestrial neighborhood as they pass across the near solar surface. Many such regions could be anticipated by a week or more if we could effectively monitor the far surface of the sun.

Helioseismic holography was proposed a decade ago (*1*) as a general diagnostic basis for local helioseismology, with the purpose of imaging local acoustic anomalies in the solar interior and on the far side. The development of holographic seismic imaging techniques for solar interior diagnostics (*2, 3*) was initially prompted by the discovery that sunspots absorb (*4, 5*) and scatter (*6*) incident acoustic waves. Phase-coherent seismic imaging opened the possibility of detecting not only local magnetic and thermal structure beneath the solar surface, but even active regions on the far side of the sun (*1*). These techniques work because the solar interior is transparent to seismic waves. We developed the basic concepts for seismic holography for these purposes (*1, 2, 7*), reviving a concept originally proposed some 15 years earlier by Roddier (*8*).

Standard holographic imaging of the near solar interior is accomplished computationally by regressing surface acoustic wave disturbances, which are determined by helioseismic observations, backward into the interior, on the basis of a computational acoustic model of the solar interior (*9*), thereby expressing a field called the coherent acoustic egression, H_+ (*10*). Generally, the surface observations that contribute to the regressed acoustic field at any given "focal point" in the image are chosen from a limited region, called the pupil of the computation. This has typically been an annulus or circular region on the model surface centered directly above the submerged focal point. In fact, waves in the 2.5- to 4.5-mHz frequency range undergo a specular reflection at the solar surface, penetrating back into the interior where they are eventually refracted back to the surface thousands of kilometers further from the source. Multiple-skip holography based on this phenomenon thus facilitates imaging of active regions from pupils far extended from the focal point. Indeed, it is even possible to extend the pupil of a holographic computation from the focal point to the opposite side of the sun. In such an application, it is the focal point that must lie on the far surface of the sun because the pupil itself must lie on the near surface in order to be directly observed. This is the principle of far-side helioseismic holography.

Standard acoustic power holography is accomplished by mapping the egression power, $|H_+|^2$, which may be integrated over time and/or temporal frequency for improved statistics. This diagnostic is sensitive to acoustic sources and absorbers, the latter of which are rendered as silhouettes. Alternatively, phase-sensitive holography (*7*) can be used to gauge travel-time perturbations, Δt, caused by refractive anomalies, or to gauge the magnetic depressions of sunspots and plages (*11*). This technique is based on phase correlations between the acoustic egression and its time-reverse counterpart, the acoustic ingression H_-, which is a coherent representation of waves that happen to be converging into the focal point, as opposed to waves emanating from it. This is the natural adaptation of time-distance correlation measurements (*12, 13*) to holographic reconstruction.

Here, we used two-skip phase-sensitive holography to map travel-time perturbations of the far side of the sun over a spectral range of 2.5 to 4.5 mHz. We analyzed a 24-hour interval of full-disk Dopplergrams, starting on 28 March 1998 07:00 UT, made by the Solar Oscillations Investigation–Michelson Doppler Imager (SOI-MDI) aboard the Solar Heliospheric Observatory (SOHO) spacecraft (*14*). We computed two-skip egression and

[1]Solar Physics Research Corporation, Tucson, AZ 85718, USA. [2]NorthWest Research Associates Inc., Colorado Research Associates Division, Boulder, CO 80301, USA.

*To whom correspondence should be addressed. E-mail: lindsey@sprc.com